

The second Kaluza-Klein neutral Higgs bosons in the minimal Universal Extra Dimension model

Sanghyeon Chang,^{*} Kang Young Lee,[†] and Jeonghyeon Song[‡]

*Division of Quantum Phases & Devices, School of Physics,
Konkuk University, Seoul 143-701, Korea*

(Dated: May 2, 2022)

Abstract

Loop-induced decay of a neutral Higgs boson into a pair of gluons or photons has great implications for the Higgs discovery at the LHC. If the Higgs boson is heavy with mass above ~ 500 GeV, however, these radiative branching ratios are very suppressed in the standard model (SM), as the new decay channels are kinematically open. We note that these radiative decays can be sizable for the heavy CP-odd second Kaluza-Klein (KK) mode of the Higgs boson, $\chi^{(2)}$, in the minimal universal extra dimension model: highly degenerate mass spectrum of the theory prohibits kinematically the dominant KK-number-conserving decays into the first KK modes of the W , Z and top quark. We find that the CP-even decay of $h^{(2)} \rightarrow gg$ is absent at one-loop level since $h^{(2)}$ couples with different mass eigenstates of $t_{1,2}^{(1)}$ while a gluon does with the same mass eigenstates. The $h^{(2)}$ production at the LHC is very suppressed. On the contrary, the process $gg \rightarrow \chi^{(2)} \rightarrow \gamma\gamma$ in an optimal scenario can be observed with manageable SM backgrounds at the LHC.

^{*} sang.chang@gmail.com

[†] kylee14214@gmail.com

[‡] jhsong@konkuk.ac.kr

I. INTRODUCTION

The universal extra dimension (UED) model [1] has recently drawn a lot of interest as it suggests solutions for proton decay [2], the number of fermion generations [3], and supersymmetry breaking [4]. Based on a flat five-dimensional (5D) spacetime, this model assumes that all the standard model (SM) fields propagate in the additional extra dimension y with size R , compactified over an S_1/Z_2 orbifold. This *universal* accessibility to the extra dimension protects the Kaluza-Klein (KK) number conservation at tree level and the KK parity conservation at loop level. This new parity invariance has two significant implications in the phenomenology. First, the compactification scale can come down as low as about 300 GeV since the contributions of the KK modes to electroweak precision observables arise only through loops. Second, the exact invariance of the KK parity allows the cold dark matter candidate, the lightest KK particle (LKP) [5].

The identity of the LKP depends crucially on the radiative corrections to the KK masses. There are two types of radiative corrections to the KK mass. The first is the bulk correction from compactification over finite distances, which is well-defined and finite. The second type corrections are from the boundary kinetic terms, which are incalculable due to unknown physics at the cutoff scale Λ . The minimal version of this model, called the mUED model, is based on the assumption that the boundary kinetic terms vanish at the cut-off scale. Then radiative corrections to the KK masses are well-defined, leading to the first KK mode of the $U(1)_Y$ gauge boson $B^{(1)}$ as the LKP [6]. Many interesting phenomenological signatures of the mUED have been studied [7].

New particle contents and their phenomenology of the UED model resemble those of a supersymmetry model with R parity conservation: all the SM particles have their heavy partner with odd parity; the decay of each heavy partner ends up with the lightest new particle (missing energy signal) plus some SM particles. There are three distinctive features of, especially, the mUED model. First, the new heavy partner has the same spin as the corresponding SM particle. In the literature, the spin discrimination in supersymmetry and UED models have been studied extensively, although very challenging at the LHC [8, 9]. The second characteristic is nearly degenerate mass spectra of new particles [9, 10]. High degeneracy in the KK masses at the same KK level makes the decay products of a heavy new particle consist of very soft SM particles with missing energy. At the LHC, this is to

be overwhelmed by QCD backgrounds. The third characteristic is the presence of *even* KK parity heavy particles, the second KK modes. The even parity allows their decay into two SM particles, which can be smoking-gun signatures of this model. In Ref. [9], it was shown that 100 fb^{-1} data of the LHC can discover the second KK modes of the Z boson and the photon through the decays into two leptons.

In this paper, we focus on the massive scalar particles with even KK parity, the second KK modes of the Higgs boson. The n -th KK modes of a $SU(2)$ doublet Higgs field consist of CP-even neutral $h^{(n)}$, CP-odd neutral $\chi^{(n)}$, and charged scalars $\phi^{\pm(n)}$. In the literature, the Higgs sector in the mUED model has been studied, mostly focused on the effects of the first KK modes. The zero mode of the Higgs boson has $\mathcal{O}(10\%)$ increase in its gluon fusion production and the $\mathcal{O}(10\%)$ decrease in the $h \rightarrow \gamma\gamma$ decay width, by the first KK mode effects through loops [11]. The phenomenological signature of $h^{(1)}$ was also discussed, concluding that the production at the LHC is suppressed because the dominant channel is through the production and subsequent decay of the first KK mode of the b quark [12]. The detection of $h^{(1)}$ is expected even more challenging because the decay products involve too soft SM particles. However the *second* KK Higgs bosons can avoid these difficulties.

In this paper we restrict ourselves to two neutral KK Higgs bosons, $\Phi^{(2)} = h^{(2)}, \chi^{(2)}$. Kaluza-Klein number conserving decay modes are tree level decays of $\Phi^{(2)}$ into $B^{(1)}B^{(1)}$, $B^{(1)}\chi^{(1)}$, $t^{(1)}\bar{t}^{(1)}$, $W^{(1)}W^{(1)}$, and $Z^{(1)}Z^{(1)}$. In the minimal model [13], however, larger radiative contributions to the KK masses of the top quark and $SU(2)$ gauge bosons prohibit these decays especially when the SM Higgs boson mass is light around 120 GeV. Even though tree level decay modes of $h^{(2)} \rightarrow B^{(1)}B^{(1)}$, $\ell^{+(1)}\ell^{-(1)}$ and $\chi^{(2)} \rightarrow \ell^{+(1)}\ell^{-(1)}$ are still kinematically allowed, the branching ratios are suppressed because of very small phase space from nearly degenerate masses and/or small lepton Yukawa couplings.

In the mUED model, therefore, the loop-induced decay of the second KK Higgs boson can be substantial. Their Feynman diagrams are illustrated in Figs. 1 and 2. As shall be shown, the vertex of $h^{(2)}-g-g$ vanishes even at one-loop level because the CP-even $h^{(2)}$ couples with different mass eigenstates of $t_{1,2}^{(1)}$ while the gluon with the same mass eigenstates. The production of the CP-even neutral Higgs boson through gluon fusion at the LHC is very suppressed. On the contrary, the decay of the CP-odd scalar $\chi^{(2)}$ into gg is substantial, which leads to sizable gluon fusion production at the LHC. In addition, $\text{BR}(\chi^{(2)} \rightarrow \gamma\gamma)$ is not extremely small as in the SM. At the LHC, the heavy CP-odd neutral Higgs boson is

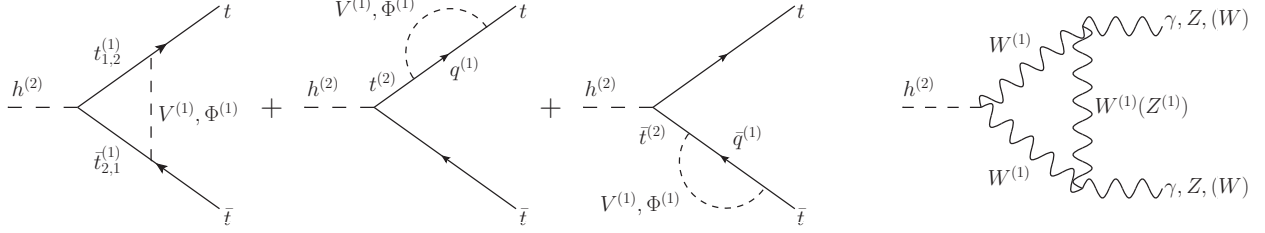


FIG. 1. The Feynman diagrams for the decay of the CP-even neutral Higgs bosons at one-loop level. $h^{(2)} \rightarrow gg$ channel is prohibited in this model. $V^{(1)}$ are first KK modes of gauge bosons and $\Phi^{(1)} = h^{(1)}, \chi^{(1)}$.

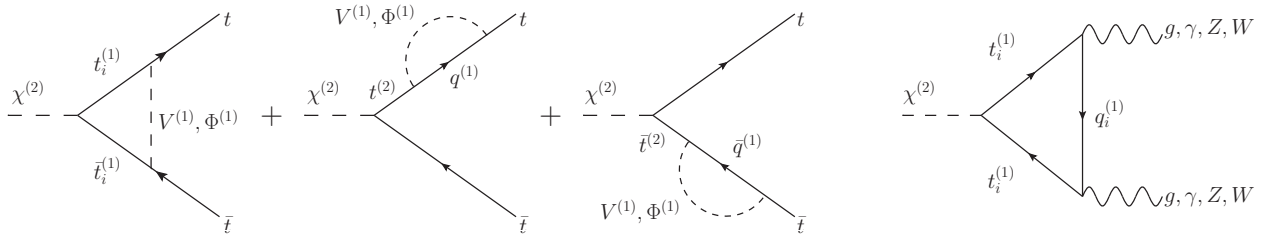


FIG. 2. The Feynman diagrams for the decay of the CP-odd neutral Higgs bosons at one-loop level.

produced through the gluon fusion, and can be detected by two hard photons. The SM backgrounds are to be shown manageable. This is our main results.

The organization of the paper is as follows. In the next section, we briefly review the model and describe the effective interactions focused on the Higgs and top quark sector. Section III deals with the production and decay of the second KK modes of the neutral Higgs bosons. For the process of $gg \rightarrow \chi^{(2)} \rightarrow \gamma\gamma$, we give details of the SM backgrounds and the kinematic cuts to see the signal in Sec. IV. We conclude in Sec. V.

II. BRIEF REVIEW OF THE MUED MODEL

The UED model is based on a flat 5D spacetime with the metric of

$$g_{MN} = \begin{pmatrix} g_{\mu\nu} & 0 \\ 0 & -1 \end{pmatrix}, \quad (1)$$

where $M, N = 0, 1, \dots, 4$, and $g_{\mu\nu} = \text{diag}(1, -1, -1, -1)$ is the 4D metric. The 5D gamma matrices are $\Gamma^M = (\gamma^\mu, i\gamma^5)$. The size of the extra dimension y is R .

In this model, all the SM fields propagate freely in the 5D bulk. The zero mode of each 5D field corresponds to the SM particle. In order to obtain chiral zero mode of a fermion from a 5D vector-like fermion field, we compactify the extra dimension on an S^1/Z_2 orbifold. We assign odd parity under the Z_2 orbifold symmetry to the zero mode fermion with wrong chirality. This extends the fermion sector to accommodate both $SU(2)$ -doublet and $SU(2)$ -singlet SM fermions. For the third generation quarks, *e.g.*, we have

$$Q_3(x, y) = \begin{pmatrix} T(x, y) \\ B(x, y) \end{pmatrix}, \quad t(x, y), \quad b(x, y). \quad (2)$$

In addition, the fifth-dimensional gauge field $V_5(x, y)$ has odd Z_2 parity.

Focused on the phenomenology of the second KK modes of the Higgs boson, we present the KK expansion of a gauge boson $V_M(x, y)$, the Higgs field $H(x, y)$, the $SU(2)$ -doublet top quark $T(x, y)$, and the $SU(2)$ -singlet top quark $t(x, y)$:

$$\begin{aligned} V_\mu(x, y) &= \frac{1}{\sqrt{\pi R}} \left[V_\mu^{(0)}(x) + \sqrt{2} \sum_{n=1}^{\infty} V_\mu^{(n)}(x) \cos \frac{ny}{R} \right], \\ V_5(x, y) &= \sqrt{\frac{2}{\pi R}} \sum_{n=1}^{\infty} V_5^{(n)}(x) \sin \frac{ny}{R}, \\ H(x, y) &= \frac{1}{\sqrt{\pi R}} \left[H^{(0)}(x) + \sqrt{2} \sum_{n=1}^{\infty} H^{(n)}(x) \cos \frac{ny}{R} \right], \\ T(x, y) &= \frac{1}{\sqrt{\pi R}} \left[T_L^{(0)}(x) + \sqrt{2} \sum_{n=1}^{\infty} \left\{ T_L^{(n)}(x) \cos \frac{ny}{R} + T_R^{(n)}(x) \sin \frac{ny}{R} \right\} \right], \\ t(x, y) &= \frac{1}{\sqrt{\pi R}} \left[t_R^{(0)}(x) + \sqrt{2} \sum_{n=1}^{\infty} \left\{ t_R^{(n)}(x) \cos \frac{ny}{R} + t_L^{(n)}(x) \sin \frac{ny}{R} \right\} \right], \end{aligned} \quad (3)$$

where $V^M = B^M, W^M, A^M$ and $f_{R,L} = (1 \pm \gamma^5)f/2$ for a fermion f . Here n is called the KK number. Note that, *e.g.*, the KK modes of $SU(2)$ -doublet top quark have both chiralities.

At tree level, the KK mass is

$$M_{KK}^{(n)} = \sqrt{M_n^2 + m_0^2}, \quad (4)$$

where $M_n = n/R$, and m_0 is the corresponding SM particle mass. All the KK mode masses are highly degenerate. In Ref. [6], it was shown that the radiative corrections generate significant changes in the KK masses. In the minimal model based on the assumption of vanishing boundary kinetic terms at the cutoff scale Λ , the corrections are well-defined and finite.

A. The Higgs sector

The 4D effective Lagrangian in the Higgs sector is obtained by integrating out the extra dimensions y :

$$\mathcal{L}_H = \frac{1}{2} \int_{-\pi R}^{\pi R} dy \left[(D_M H)^\dagger D^M H + \mu^2 H^\dagger H - \frac{\lambda_{h5}}{2} (H^\dagger H)^2 \right], \quad (5)$$

where D_M is the covariant derivative given by $D_M H = (\partial_M - \frac{i}{2} g_5 \tau^i W_M^i - \frac{i}{2} g_5' B_M)$. The 4D SM Higgs boson interaction is recovered if $g^{(l)} = g_5^{(l)}/\sqrt{\pi R}$ and $\lambda_h = \lambda_{h5}/\sqrt{\pi R}$. The Lagrangian in Eq. (5) yields the following 4D potential of the Higgs boson:

$$V_{\text{eff}} = -\mu^2 H^{(0)\dagger} H^{(0)} + \frac{\lambda_h}{2} (H^{(0)\dagger} H^{(0)})^2 \quad (6)$$

$$+ \sum_{n=1}^{\infty} (M_n^2 - \mu^2) H^{(n)\dagger} H^{(n)} + \frac{1}{4} \lambda_h \sum_{n,m,\ell,k=1}^{\infty} H^{(n)\dagger} H^{(m)} H^{(\ell)\dagger} H^{(k)} \Delta_{n,m,\ell,k}^2,$$

where

$$\Delta_{n,m,\ell,k}^2 = \delta_{k,\ell+n+m} + \delta_{\ell,n+m+k} + \delta_{n,m+k+\ell} + \delta_{m,n+k+\ell} + \delta_{k+m,n+\ell} + \delta_{k+n,m+\ell} + \delta_{k+\ell,m+n}. \quad (7)$$

Positive μ^2 (or negative mass squared) generates non-zero vacuum expectation value (VEV) for the SM Higgs boson $H^{(0)}$, which triggers the electroweak symmetric breaking. However the condition $R^{-1} > \mu$ leads to positive mass squared parameters for all the KK Higgs bosons: the KK Higgs bosons do not have non-zero VEV.

The n -th KK mode of the $SU(2)$ -doublet Higgs boson is

$$H^{(n)}(x) = \begin{pmatrix} \phi^{(n)+} \\ \frac{1}{\sqrt{2}} (h^{(n)} + i\chi^{(n)}) \end{pmatrix}, \quad (8)$$

where $h^{(n)}$ and $\chi^{(n)}$ are the CP-even and CP-odd neutral scalar fields, respectively. The mass eigenstate of CP-odd scalar $\chi_Z^{(n)}$ is a linear combination of $\chi^{(n)}$ and the fifth component of the n -th KK mode of the Z boson, $Z^{5(n)}$:

$$\chi_Z^{(n)} = \frac{M_n \chi^{(n)} + m_Z Z^{5(n)}}{\sqrt{M_n^2 + m_Z^2}} \equiv \cos \theta_\chi^{(n)} \chi^{(n)} + \sin \theta_\chi^{(n)} Z^{5(n)}. \quad (9)$$

Its orthogonal combination is the Goldstone mode $G_Z^{(n)}$ for the $Z_\mu^{(n)}$ [11]. Note that $\chi_Z^{(n)}$ and $Z^{(n)}$ have the same mass at tree level. The KK masses of neutral Higgs bosons are

$$m_{h^{(n)}}^2 = M_n^2 + m_h^2 + \delta m_{H^{(n)}}^2, \quad (10)$$

$$m_{\chi^{(n)}}^2 = M_n^2 + m_Z^2 + \delta m_{H^{(n)}}^2, \quad (11)$$

where $m_h^2 = \lambda_h v^2$ and $v \approx 246$ GeV is the VEV of the SM Higgs boson. The radiative mass correction to n -th KK scalar masses is

$$\delta m_{H^{(n)}}^2 = M_n^2 \left(\frac{3}{2}g^2 + \frac{3}{4}g'^2 - \lambda_h \right) \frac{1}{16\pi^2} \ln \frac{\Lambda^2}{\mu^2}, \quad (12)$$

where μ is the regularization scale [6]. For the second KK mode production, we put $\mu = 2R^{-1}$ [12].

B. The top quark sector

Due to large top quark mass, there is non-negligible mixing between the KK modes of $SU(2)$ -doublet and $SU(2)$ -singlet top quarks in the same KK level. Their 4D effective Lagrangian is

$$\mathcal{L}_t = \frac{1}{2} \int_{-\pi R}^{\pi R} dy \left[i\bar{T} \not{D} T + i\bar{t} \not{D} t - \left(\lambda_{t5} \bar{Q}_3 \tilde{H} t + H.c. \right) \right], \quad (13)$$

where $\tilde{H} = i\sigma_2 H^*$. As the zero mode of the Higgs boson develops non-zero VEV of v , the mass matrix of the KK top quark becomes non-diagonal. Including the radiative corrections to the mass, the n -th KK mass term for the top quark is

$$- \mathcal{L}_{\text{mass}} = \sum_{n=1}^{\infty} \left(\bar{T}_L^{(n)}, \bar{t}_L^{(n)} \right) \begin{pmatrix} M_n + \delta m_{T^{(n)}} & m_t \\ m_t & -M_n - \delta m_{t^{(n)}} \end{pmatrix} \begin{pmatrix} T_R^{(n)} \\ t_R^{(n)} \end{pmatrix}, \quad (14)$$

where $\delta m_{T^{(n)}}$ and $\delta m_{t^{(n)}}$ are, respectively, the radiative corrections to the $SU(2)$ -doublet and $SU(2)$ -singlet top quarks, given by [6]

$$\begin{aligned} \delta m_{T^{(n)}} &= \frac{M_n}{16\pi^2} \left(3g_s^2 + \frac{27}{16}g^2 + \frac{1}{16}g'^2 - \frac{3}{4}y_t^2 \right) \ln \frac{\Lambda^2}{\mu^2}, \\ \delta m_{t^{(n)}} &= \frac{M_n}{16\pi^2} \left(3g_s^2 + g'^2 - \frac{3}{2}y_t^2 \right) \ln \frac{\Lambda^2}{\mu^2}, \end{aligned} \quad (15)$$

where $y_t = m_t/v$. The KK mass of the $SU(2)$ -doublet top quark $T^{(n)}$ has larger radiative corrections than that of the $SU(2)$ -singlet top quark $t^{(n)}$.

Two mass eigenstates of the n -th KK mode are denoted by $t_1^{(n)}$ and $t_2^{(n)}$. Here $t_1^{(n)}$ is the lighter mass eigenstate. The mass eigenstates are related with electroweak eigenstates $t^{(n)}$

and $T^{(n)}$ through the mixing angle $\theta_t^{(n)}$:

$$\begin{aligned} \begin{pmatrix} t_{1R}^{(n)} \\ t_{2R}^{(n)} \end{pmatrix} &= \begin{pmatrix} \cos \frac{\theta_t^{(n)}}{2} & -\sin \frac{\theta_t^{(n)}}{2} \\ \sin \frac{\theta_t^{(n)}}{2} & \cos \frac{\theta_t^{(n)}}{2} \end{pmatrix} \begin{pmatrix} t_R^{(n)} \\ T_R^{(n)} \end{pmatrix}, \\ \begin{pmatrix} t_{1L}^{(n)} \\ t_{2L}^{(n)} \end{pmatrix} &= \begin{pmatrix} \cos \frac{\theta_t^{(n)}}{2} & -\sin \frac{\theta_t^{(n)}}{2} \\ -\sin \frac{\theta_t^{(n)}}{2} & -\cos \frac{\theta_t^{(n)}}{2} \end{pmatrix} \begin{pmatrix} t_L^{(n)} \\ T_L^{(n)} \end{pmatrix}. \end{aligned} \quad (16)$$

The mixing angle $\theta_t^{(n)}$ is

$$\tan \theta_t^{(n)} = \frac{m_t}{M_n + \frac{\delta m_{T^{(n)}} + \delta m_{t^{(n)}}}{2}}, \quad (17)$$

and the physical masses are, to a good approximation,

$$m_{t_1^{(n)}} = \sqrt{(M_n + \delta m_{t^{(n)}})^2 + m_t^2}, \quad m_{t_2^{(n)}} = \sqrt{(M_n + \delta m_{T^{(n)}})^2 + m_t^2}. \quad (18)$$

III. THE LHC REACH FOR THE SECOND KK HIGGS BOSONS

The 4D interaction Lagrangian for $h^{(2)}$ is

$$\begin{aligned} \mathcal{L}_{h^{(2)}} &= -y_{t(2)} h^{(2)} \bar{t} t + i y_{t(2)} \chi^{(2)} \bar{t} \gamma_5 t - y_t h^{(2)} \left(\bar{t}_1^{(1)} t_2^{(1)} + \bar{t}_2^{(1)} t_1^{(1)} \right) \\ &\quad + \frac{g'^2 v}{4} h^{(2)} B_\mu^{(1)} B^{(1)\mu} + \frac{g^2 v}{2\sqrt{2}} h^{(2)} W_\mu^{(1)\dagger} W^{(1)\mu} + \frac{g^2 v}{2\sqrt{2}} h^{(2)} Z_\mu^{(1)\dagger} Z^{(1)\mu} \\ &\quad + \frac{g'}{2\sqrt{2}} \left[(\partial^\mu \chi^{(1)}) h^{(2)} - \chi^{(1)} \partial^\mu h^{(2)} \right] B_\mu^{(1)}, \end{aligned} \quad (19)$$

and that for $\chi_Z^{(2)}$ is

$$\begin{aligned} \mathcal{L}_{\chi_Z^{(2)}} &= -i y_t \cos \theta_\chi^{(2)} \chi_Z^{(2)} \left[\sin \theta_t^{(1)} \left(\bar{t}_1^{(1)} \gamma^5 t_1^{(1)} + \bar{t}_2^{(1)} \gamma^5 t_2^{(1)} \right) + \cos \theta_t^{(1)} \left(\bar{t}_1^{(1)} t_2^{(1)} - \bar{t}_2^{(1)} t_1^{(1)} \right) \right] \\ &\quad - i \frac{g}{\sqrt{2}} \sin \theta_\chi^{(2)} \chi_Z^{(2)} \bar{t}_2^{(1)} \gamma_5 t_2^{(1)} \\ &\quad - e Q_t A_\mu^{(0)} \left[\bar{t}_1^{(1)} \gamma^\mu t_1^{(1)} + \bar{t}_2^{(1)} \gamma^\mu t_2^{(1)} \right] - g_s \left[\bar{t}_1^{(1)a} \gamma^\mu \mathbf{G}_\mu^{(0)} t_1^{(1)b} + \bar{t}_2^{(1)a} \gamma^\mu \mathbf{G}_\mu^{(0)} t_2^{(1)b} \right], \end{aligned} \quad (20)$$

where $\mathbf{G}_\mu^{(0)} \equiv G_\mu^{(0)c} T_{ab}^c$ and a, b, c are the color indices. We have shown interactions to leading order in the small KK mixing angle $\theta_{t,\chi}^{(n)}$. Note that the second line of Eq. (20) is from the interaction of Z^5 through the mixing in Eq. (9). Since the second KK mixing angle $\theta_\chi^{(2)}$ is smaller than the first KK mixing angle $\theta_\chi^{(1)}$, the effect of the second line of Eq. (20) is subleading. The vertex of $h^{(2)} \bar{t} t$ at one-loop level is [14]

$$y_{t(2)} = \frac{y_t}{48\sqrt{2}\pi^2} \left(16g_s^2 - \frac{39}{4}g^2 + \frac{4}{3}g'^2 - 9y_t^2 + 3\lambda_h \right) \ln \frac{\Lambda}{\mu}. \quad (21)$$

Similar expressions for other KK fermions such as the KK tau lepton can be inferred with the replacement of $\theta_\tau \sim m_\tau R \ll 1$.

The tree level decay rates of CP-even $h^{(2)}$ are

$$\Gamma(h^{(2)} \rightarrow V^{(1)}V^{(1)}) = \mathcal{S} \frac{g_{H_2 V_1 V_1}^2}{64\pi} \frac{1}{m_{h^{(2)}}} \frac{1 - 4x_V^2 + 12x_V^4}{x_V^4} \sqrt{1 - 4x_V^2}, \quad (22)$$

$$\Gamma(h^{(2)} \rightarrow \chi^{(1)}B^{(1)}) = \frac{g'^2}{128\pi} \frac{m_{h^{(2)}}^3}{m_{B^{(1)}}^2} \lambda^{3/2} \left(x_{\chi^{(1)}}^2, x_{B^{(1)}}^2 \right), \quad (23)$$

$$\Gamma(h^{(2)} \rightarrow t_1^{(1)}\bar{t}_2^{(1)}) = N_C y_t^2 \frac{m_{h^{(2)}}}{16\pi} [1 - (x_{t_1} + x_{t_2})]^{3/2} [1 - (x_{t_1} - x_{t_2})]^{1/2}, \quad (24)$$

where $V_\mu^{(1)} = B_\mu^{(1)}, W_\mu^{(1)}, Z_\mu^{(1)}$, \mathcal{S} is the symmetric factor ($\mathcal{S} = 1/2$ for $V_\mu^{(1)} = B_\mu^{(1)}, Z_\mu^{(1)}$ and $\mathcal{S} = 1$ for $V_\mu^{(1)} = W_\mu^{(1)}$), $x_i = m_i/m_{h^{(2)}}$, and $\lambda(a, b) = 1 + a^2 + b^2 - 2a - 2b - 2ab$. The vertices of $h^{(2)}-V^{(1)}-V^{(1)}$ are

$$g_{H_2 B_1 B_1} = \frac{g'^2}{2} v, \quad g_{H_2 Z_1 Z_1} = g_{H_2 W_1 W_1} = \frac{g^2}{2\sqrt{2}} v. \quad (25)$$

Note that $g_{H_2 Z_1 Z_1}$ and $g_{H_2 W_1 W_1}$ are the same to leading order because of very small KK Weinberg angle [6]. Compared to the SM coupling of h - W - W , $g_{H_2 W_1 W_1}$ has additional factor of $1/\sqrt{2}$.

At one-loop level, $h^{(2)}$ decays into a pair of top quarks, and a pair of photons. Their decay rates are

$$\begin{aligned} \Gamma(h^{(2)} \rightarrow t\bar{t}) &= N_C y_{t^{(2)}}^2 \frac{m_{h^{(2)}}}{8\pi} (1 - 4x_t^2)^{3/2}, \\ \Gamma(h^{(2)} \rightarrow \gamma\gamma) &= \frac{g^2 \alpha^2 m_W^2}{128\pi^3 m_{h^{(2)}}} \left| \hat{\mathcal{A}}_1^H(\tau_{W^{(1)}}) \right|^2, \end{aligned} \quad (26)$$

where $\tau_i = 1/(4x_i^2) = m_{h^{(2)}}^2/4m_i^2$. The normalized amplitude for spin-1 particles is given by

$$\hat{\mathcal{A}}_1^H(\tau) = - [2\tau^2 + 3\tau + 3(2\tau - 1)f(\tau)] \tau^{-1}, \quad (27)$$

where the universal scalar function $f(\tau)$ is

$$f(\tau) = \begin{cases} \arcsin^2 \sqrt{\tau} & \text{if } \tau \leq 1, \\ -\frac{1}{4} \left[\ln \frac{1 + \sqrt{1 - \tau^{-1}}}{1 - \sqrt{1 - \tau^{-1}}} - i\pi \right]^2 & \text{if } \tau > 1. \end{cases} \quad (28)$$

The CP-odd $\chi^{(2)}$ has only radiative decays because of its small mass both in the light

and heavy m_h cases. The decay rates are

$$\begin{aligned}\Gamma(\chi^{(2)} \rightarrow t\bar{t}) &= N_C y_{t(2)}^2 \frac{m_{\chi^{(2)}}}{8\pi} (1 - 4x_t^2)^{1/2}, \\ \Gamma(\chi^{(2)} \rightarrow \gamma\gamma) &= \frac{G_F \alpha^2 m_{\chi^{(2)}}^3}{128\sqrt{2}\pi^3} \left(\frac{m_t}{m_{t(1)}} \right)^2 \left| \sum_{i=t_1^{(1)}, t_2^{(1)}} N_C Q_t^2 \sin \theta \mathcal{A}_{1/2}^A(\tau_i) \right|^2, \\ \Gamma(\chi^{(2)} \rightarrow gg) &= \frac{G_F \alpha_s^2 m_{\chi^{(2)}}^3}{36\sqrt{2}\pi^3} \left(\frac{m_t}{m_{t(1)}} \right)^2 \left| \frac{3}{4} \sum_{i=t_1^{(1)}, t_2^{(1)}} \sin \theta \mathcal{A}_{1/2}^A(\tau_i) \right|^2.\end{aligned}\tag{29}$$

The amplitude for spin-1/2 particles is

$$\mathcal{A}_{1/2}^A(\tau) = 2\tau^{-1} f(\tau),\tag{30}$$

where $f(\tau)$ is given in Eq. (28). For more complicated expressions of $\Gamma(h^{(2)}/\chi^{(2)} \rightarrow WW, ZZ, Z\gamma)$ we refer the reader to Ref. [15, 16].

Brief comments on the lower bounds on R^{-1} are in order here. Indirect observables put rather strong constraint on R^{-1} . Electroweak precision data with the subleading new physics contributions and two-loop corrections to the SM ρ parameter leads to $R^{-1} \gtrsim 600$ (300) GeV for $m_h = 115$ (600) GeV at 90% confidence level [17]. In addition, the $B \rightarrow X_s \gamma$ branching ratio constrains this model more seriously since the mUED KK modes interfere destructively with the SM amplitude [18]. At the 95% (99%) confidence level, the bound is $R^{-1} \gtrsim 600$ (300) GeV. Since we are focused on the direct probe of this model, we take flexible parameter space of $R^{-1} \in [350, 600]$ GeV as marginally allowed by indirect constraints, which is commonly searched in the literature [19]. For the Higgs boson mass, we take two cases, the light Higgs boson case of $m_h = 120$ GeV and the heavy Higgs boson case of $m_h = 600$ GeV.

At tree level, only the KK-number-conserving interactions are possible: a second KK mode mainly decays into two first KK mode particles. The mass spectra of the first and second KK modes determine the kinematic permission of each decay channel. In Table I, we show the KK masses of the first KK modes of CP-odd Higgs boson, gauge bosons, top quark and tau lepton as well as the second KK modes of the CP-even and CP-odd Higgs boson in the mUED model. We set $\Lambda R = 20$, and take $R^{-1} = 350, 400, 500$ GeV for $m_h = 120, 600$ GeV cases.

The SM Higgs boson mass affects most drastically the KK mass of the Higgs boson. As in Eq. (4), the tree level KK mass consists of the geometrical mass and the corresponding SM

TABLE I. The masses of KK states which can be involved in the second KK state of the Higgs boson. We include one-loop radiative corrections and fix $\Lambda R = 20$ and $m_h = 120$ GeV. Masses and the decay rate are in units of GeV.

R^{-1}	m_h	$h^{(2)}$	$\chi_Z^{(2)}$	$\chi_Z^{(1)}$	$B^{(1)}$	$W^{\pm(1)}$	$t_1^{(1)}$	$t_2^{(1)}$	$\tau_1^{(1)}$	$\tau_2^{(1)}$
350	120	715.9	711.7	365.3	351.4	377.5	410.9	428.4	354.0	360.0
	600	881.2	651.8	327.0						
400	120	815.7	811.8	414.5	401.3	429.2	459.2	479.2	404.5	411.4
	600	950.8	699.0	370.3						
500	120	1015.4	1012.4	513.5	500.9	533.2	558.1	583.0	505.7	514.2
	600	1100.0	926.5	457.8						

particle mass. In the heavy SM Higgs boson case, large m_h makes the mass of $h^{(2)}$ much larger than $M_2(= 2R^{-1})$, as in Eq. (4): the KK mass degeneracy is broken for $h^{(2)}$. An interesting observation is that large m_h or large Higgs quartic coupling λ_h makes *negative* contributions through the radiative corrections as in Eq. (12). This negative $\delta m_{H^{(n)}}^2$ contribution applies to the CP-odd $\chi^{(n)}$ identically, while the tree level KK mass of $\chi^{(n)}$ has the SM Z boson mass, not the SM Higgs boson mass. Therefore, the KK modes of the CP-odd Higgs boson become lighter as m_h increases.

In the light Higgs boson case ($m_h = 120$ GeV), tree level decays of the second KK Higgs bosons are $h^{(2)} \rightarrow B^{(1)}B^{(1)}$, $h^{(2)}/\chi^{(2)} \rightarrow \ell^{(1)}\ell^{(1)}$, and $h^{(2)}/\chi^{(2)} \rightarrow \ell^{(2)}\ell$. All other decay channels are kinematically closed, and CP-*odd* $\chi^{(2)}$ cannot decay into two $B^{(1)}$'s. In addition, leptonic decay modes are numerically negligible. Even the most dominant leptonic decay mode has $\Gamma(h^{(2)} \rightarrow \tau^{(1)}\tau^{(1)}) \sim \text{keV}$, which is very suppressed by small Yukawa coupling of the tau lepton and the very limited kinematic phase space because of $m_{\tau^{(1)}} \approx 0.5m_{h^{(2)}}$. Another tree level decay mode, $h^{(2)}/\chi^{(2)} \rightarrow \ell_R^{(2)}\ell$, is also very suppressed because of the same reasons. For definiteness, we present the masses of the second KK tau leptons and $\Gamma(h^{(2)} \rightarrow \tau_R^{(2)}\tau)$ with the fixed $R\Lambda = 20$ and $m_h = 120$ GeV:

R^{-1}	$m(\tau_R^{(2)})$	$m(\tau_L^{(2)})$	$\Gamma(h^{(2)} \rightarrow \tau_R^{(2)}\tau)$
350 GeV	706.1 GeV	715.4 GeV	20.2 keV
400 GeV	807.0 GeV	817.6 GeV	18.0 keV
500 GeV	1008.7 GeV	1021.9 GeV	13.9 keV

(31)

Thus the dominant tree level decay mode of $h^{(2)}$ in the light Higgs boson case is into a pair of LKP's. Since $B^{(1)}$ is a CDM candidate in this model, this decay does not leave any track in the detector, and appears as a missing energy signal.

At one-loop level, the KK number conservation is broken while the KK-parity is still preserved. Thus the second KK mode of the Higgs boson can decay into two SM particles through loops mediated by first KK modes. First $h^{(2)}$ and $\chi^{(2)}$ can decay into a pair of top quarks through the triangle diagram (see Figs. 1 and 2). As shall be shown, this $t\bar{t}$ decay mode is dominant for both $h^{(2)}$ and $\chi^{(2)}$. Unfortunately the huge SM $t\bar{t}$ backgrounds obstruct the observation of the signal. Second types of radiative decays are into a SM gauge boson pair of WW , ZZ , $Z\gamma$, $\gamma\gamma$ and gg . For the decay of $h^{(2)}$ and $\chi^{(2)}$ these decays are through the first KK gauge boson and the first KK top quarks respectively.

The radiative decays of $\Phi^{(2)}(= h^{(2)}, \chi^{(2)})$ into a pair of gluons or photons require more detailed discussion. The decay $h^{(2)} \rightarrow gg$ is through the loop mediated by the first KK modes of the top quark, as illustrated in Figs.1 and 2. However the effective vertex of $h^{(2)}-g-g$ at one-loop level vanishes because the CP-even scalar $h^{(2)}$ does not interact with two identical mass eigenstates of the first KK top quarks as can be seen in Eq. (19). Since the photon and gluon couple with $t_i^{(1)}\bar{t}_i^{(1)}$, the decay of $h^{(2)} \rightarrow gg$ and thus the gluon fusion production of $h^{(2)}$ are not possible. On the contrary, the CP-odd scalar $\chi^{(2)}$ couples with the same mass eigenstates of the KK top quarks, although the coupling strength is suppressed by the KK top mixing angle of the order of m_t/M_1 . The decay of $\chi^{(2)} \rightarrow gg$ and its gluon fusion production are feasible at the LHC.

If the SM Higgs boson is heavy, *e.g.*, $m_h = 600$ GeV, the second KK mode of CP-even Higgs boson becomes also heavy as in Table I. Now $h^{(2)} \rightarrow W^{(1)}W^{(1)}, Z^{(1)}Z^{(1)}$ decay mode is open. Another interesting decay mode is into $\chi^{(1)}B^{(1)}$, as suggested by the third line of Eq. (19). This mode is dominant since the vertex of $h^{(2)}-\chi^{(1)}-B^{(1)}$ is proportional to the $h^{(2)}$ mass, while that of $h^{(2)}-W^{(1)}-W^{(1)}$ is proportional to the SM gauge boson mass. Finally $h^{(2)} \rightarrow t_{1,2}^{(1)}\bar{t}_{2,1}^{(1)}$ is also kinematically allowed.

In Fig. 3, we present the branching ratio of $h^{(2)}$ as a function of its mass in the light SM Higgs boson case ($m_h = 120$ GeV). The decay into $t\bar{t}$ is dominant because of the large Yukawa coupling and strong coupling as in Eq. (21). The next dominant decay mode is KK-number conserving decay of $h^{(2)} \rightarrow B^{(1)}B^{(1)}$. This invisible branching ratio is about 1%. Narrow kinematic phase space from the degenerate mass spectrum suppresses this decay.

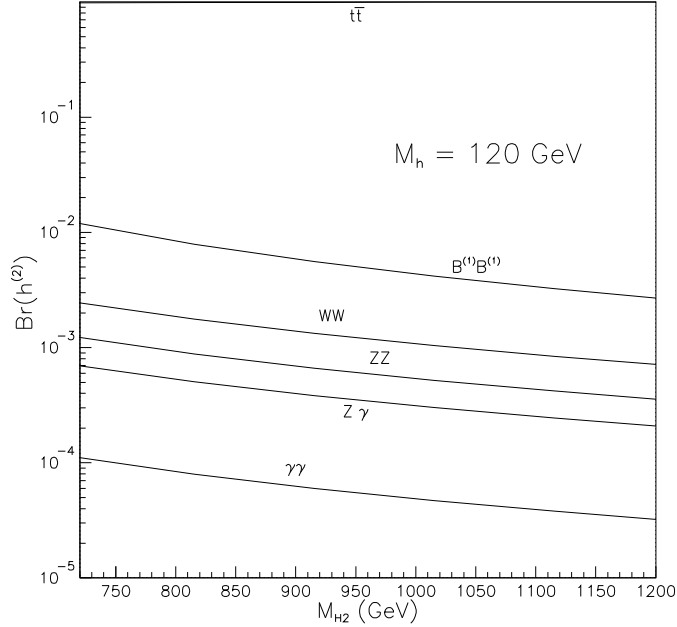


FIG. 3. The branching ratios of the CP-even second KK neutral Higgs boson, $h^{(2)}$, as functions of its mass. We set $m_h = 120$ GeV and $\Lambda R = 20$.

Following decay modes are WW , ZZ , $Z\gamma$, and $\gamma\gamma$.

Figure 4 presents the branching ratios of $h^{(2)}$ in the heavy SM Higgs boson case. Large m_h enhances $h^{(2)}$ mass significantly. In this case, the decay into $\chi^{(1)}B^{(1)}$ is the most dominant one. This can be understood by the large vertex $h^{(2)}-\chi^{(1)}-B^{(1)}$ which is proportional to the heavy $h^{(2)}$ mass, while the vertex $h^{(2)}-V^{(1)}-V^{(1)}$ is proportional to the SM gauge boson $m_{W,Z}$. The produced $\chi^{(1)}B^{(1)}$ decays through $h^{(2)} \rightarrow \chi^{(1)}B^{(1)} \rightarrow h^*B^{(1)}B^{(1)} \rightarrow \bar{b}bB^{(1)}B^{(1)}$. At the LHC, this signal is overwhelmed by QCD backgrounds. The next dominant decay mode is into a top quark pair, which becomes more significant as $m_{h^{(2)}}$ increases. Kaluza-Klein number conserving modes into $W^{(1)}W^{(1)}$, $Z^{(1)}Z^{(1)}$, $B^{(1)}B^{(1)}$, and $t^{(1)}\bar{t}^{(1)}$ follow. Note that for $R^{-1} > 420$ GeV and $m_h = 600$ GeV, $h^{(2)} \rightarrow t^{(1)}\bar{t}^{(1)}$ is not kinematically allowed. Radiative decays into a pair of SM gauge bosons are very suppressed.

The CP-odd Higgs boson $\chi^{(2)}$ does not have large enough mass for KK-number-conserving decays. Only radiative decays are allowed. This pattern remains the same for the heavy Higgs boson case because the $\chi^{(2)}$ mass decreases with increasing m_h as discussed before. In

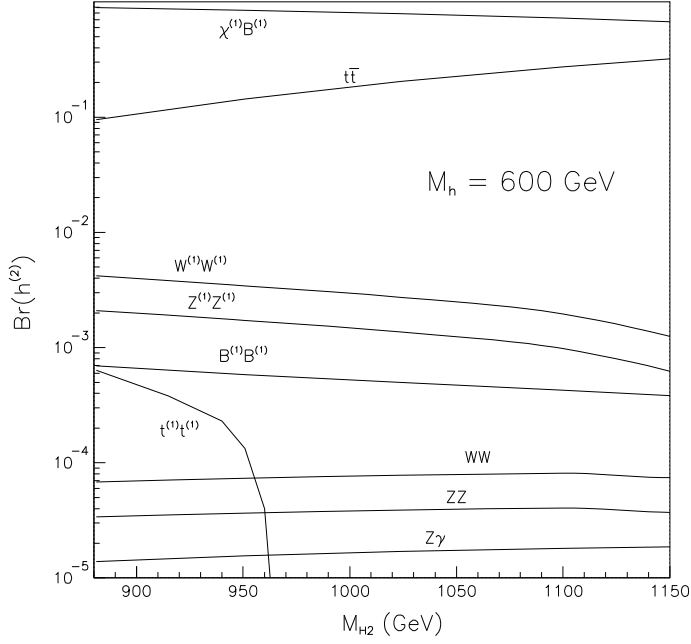


FIG. 4. The branching ratios of the CP-even second KK neutral Higgs bosons, $h^{(2)}$, as functions of its mass. We set $m_h = 600$ GeV and $\Lambda R = 20$.

Fig. 5, we present the branching ratios of $\chi^{(2)}$ only in the light m_h case. The leading decay mode of $\chi^{(2)}$ is into a pair of top quarks. The next dominant one is into a gluon pair with $\text{BR}(\chi^{(2)} \rightarrow gg) \approx 20 - 40\%$. We expect quite efficient production of $\chi^{(2)}$ through the gluon fusion at the LHC. Decays into a pair of the SM gauge bosons follow, in the order of ZZ , $\gamma\gamma$, $Z\gamma$, and WW . For the detection of $\chi^{(2)}$ at the LHC, the $\gamma\gamma$ mode is expected to be most efficient. The dominant decay mode into $t\bar{t}$ suffers from large SM background with the cross section of ~ 900 pb [21]. Other channels into W 's or Z 's have additional suppression from their small branching ratios of leptonic decay. The decay into $\gamma\gamma$ has the branching ratio of $\sim 0.1\%$. As shall be seen below, $gg \rightarrow \chi^{(2)} \rightarrow \gamma\gamma$ in an optimal scenario has a good chance to be observed at the LHC.

In all three cases of Figs. 3–5, $t\bar{t}$ decay mode is dominant, even though it is generated at one-loop level. Suppressed KK-number-conserving decays are attributed to degenerate masses and thus small phase space. Much smaller branching ratios of the decays into the SM gauge bosons than that into $t\bar{t}$ can be understood by two factors. First, the coupling

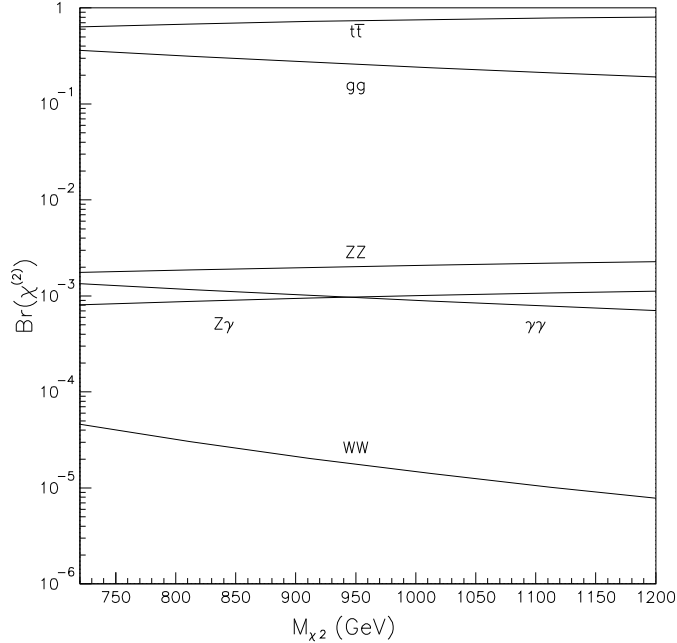


FIG. 5. The branching ratios of the CP-odd second KK neutral Higgs bosons, $\chi^{(2)}$, as functions of its mass. We set $m_h = 120 \text{ GeV}$ and $\Lambda R = 20$.

strength of $h^{(2)}-t\bar{t}$, of which the dominant part is proportional to $y_t g_s^2$, is much larger than that of $h^{(2)}-V_\mu V_\nu$ which is proportional to g^3 . Second the decay amplitude of $h^{(2)} \rightarrow t\bar{t}$ is characterized by $m_{h^{(2)}}$ while that of $h^{(2)} \rightarrow V_\mu V_\nu$ by m_W .

In Fig. 6 we compare the total decay widths of $\chi^{(2)}$ and $h^{(2)}$ with that of the SM Higgs boson. We set $\Lambda R = 20$, and $m_h = 120, 600 \text{ GeV}$ for $h^{(2)}$. The kinematic closure of many KK-number-conserving decays suppresses their total decay widths quite a lot. The second KK Higgs bosons, even though very heavy, are not obese like the SM one. At a collider, they are expected to appear as resonances.

At the LHC, the most promising production is that of $\chi^{(2)}$ through gluon fusion process, $pp \rightarrow gg \rightarrow \chi^{(2)}$. The production cross section at the parton level is given by

$$\hat{\sigma}(gg \rightarrow \chi^{(2)}) = \frac{4\pi^2}{9m_{\chi^{(2)}}^3} \Gamma(\chi^{(2)} \rightarrow gg). \quad (32)$$

Figure 7 shows the production cross section $\sigma(pp \rightarrow gg \rightarrow \chi^{(2)})$ as a function of R^{-1} at the LHC with $\sqrt{s} = 14 \text{ TeV}$. We take two cases of $m_h = 120, 600 \text{ GeV}$. For the parton distribution function, we have used the MRST 99 [22]. In the heavy SM Higgs boson case,

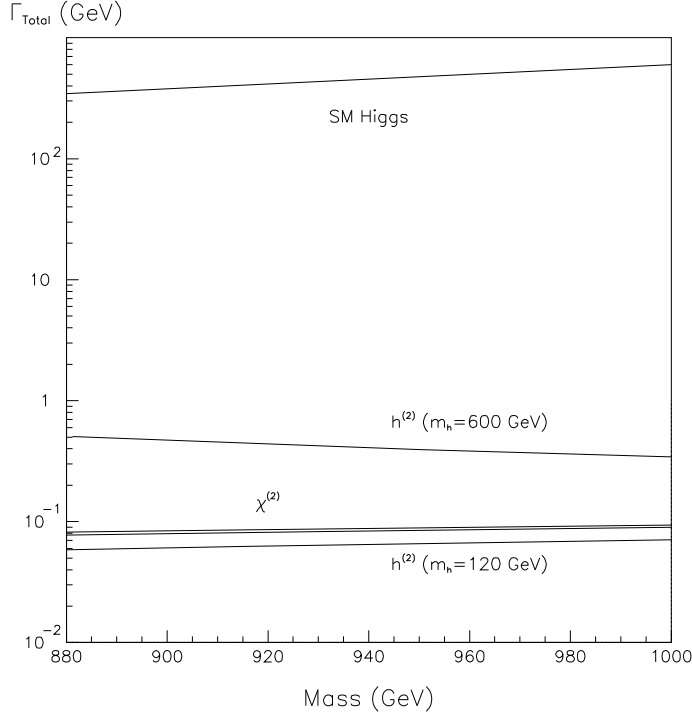


FIG. 6. The total decay widths of $\chi^{(2)}$, $h^{(2)}$ and the SM Higgs boson with respect to their masses.

the production cross of $pp \rightarrow gg \rightarrow \chi^{(2)}$ is larger than that in the light Higgs case with the given R^{-1} . It is mainly because of lighter $\chi^{(2)}$ mass with large m_h , as shown in Table I. In addition, large m_h case is much less constrained by indirect observables such as electroweak precision data and $B \rightarrow X_s \gamma$: for $m_h = 600$ GeV, $R^{-1} > 300$ GeV and $m_{\chi^{(2)}} > 560$ GeV.

Assuming the LHC integrated luminosity of 100 fb^{-1} , about 10,000 events of $\chi^{(2)}$ production are expected for $R^{-1} = 500$ GeV. The most of $\chi^{(2)}$'s decay into a pair of top quark or gluon jets, which suffers from huge QCD backgrounds. For heavier $\chi^{(2)}$ with mass above 1 TeV, top tagging becomes efficient and it can be a good channel to test the model. For $R^{-1} < 500$ GeV, however, top tagging efficient drops too much [23, 24]. The next dominant decay modes are into ZZ , $Z\gamma$ and $\gamma\gamma$. Considering small leptonic branching ratio of Z , detection efficiency for the Z boson is low. Thus $\chi^{(2)} \rightarrow \gamma\gamma$ is most promising decay channel to test the mUED model for $300 \text{ GeV} \leq R^{-1} \leq 600 \text{ GeV}$. Since the branching ratio of $\text{BR}(\chi^{(2)} \rightarrow \gamma\gamma)$ is about 0.1%, we will have dozens of events of $\gamma\gamma$ pair from the $\chi^{(2)}$ decays.

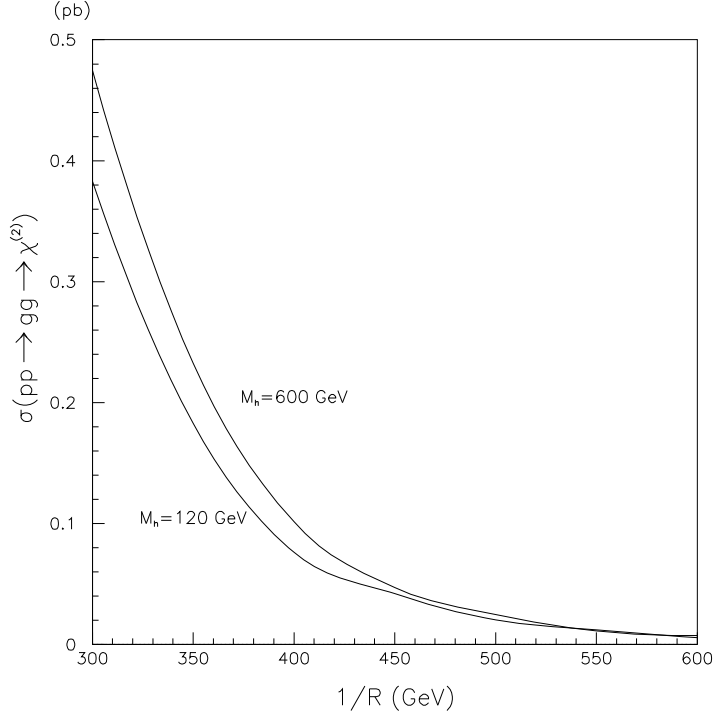


FIG. 7. The cross section of $pp \rightarrow gg \rightarrow \chi^{(2)}$ at the LHC with respect to the mass of $\chi^{(2)}$.

For the optimal case of the detection of $pp \rightarrow gg \rightarrow \chi^{(2)} \rightarrow \gamma\gamma$, we take

$$m_h = 600 \text{ GeV}, \quad R^{-1} = 300 \text{ GeV}, \quad m_{\chi^{(2)}} = 560 \text{ GeV}. \quad (33)$$

We adopt the K-factor of 1.3, which represents the enhancement from higher order QCD processes [25]. Then the $\chi^{(2)}$ production cross section at the LHC is about 0.61 pb. With $\text{Br}(\chi^{(2)} \rightarrow \gamma\gamma) \approx 10^{-3}$ and the integrated luminosity of 100 fb^{-1} , $\sigma_{\chi^{(2)}} \text{Br}(\chi^{(2)} \rightarrow \gamma\gamma)$ has about 60 events. And the invariant mass distributions of two photons will show a resonant peak at the $\chi^{(2)}$ mass. This special decay of $\chi^{(2)} \rightarrow \gamma\gamma$ can be a smoking gun signature to discriminate the mUED from SM or minimal supersymmetric standard model (MSSM) type heavy Higgs decay [15].

IV. BACKGROUND STUDY

The photon events suffer from huge backgrounds from QCD processes. Here, we estimate the backgrounds at the LHC with appropriate kinematic cuts to check the significance of our

signal. In the ordinary $H \rightarrow \gamma\gamma$ analysis of the SM, the background events are classified into two groups, the irreducible backgrounds coming from two isolated photons at the parton level and the reducible backgrounds including at least one fake photon. Fake photons are mostly from the decays of π^0 's. For the SM Higgs boson with mass about 150 GeV, the two types of backgrounds are compatible to each other [20]. For the heavy Higgs boson with mass $\gtrsim 500$ GeV, however, the irreducible backgrounds are negligible since their subprocesses such as $pp \rightarrow q\bar{q} \rightarrow \gamma\gamma$ and $pp \rightarrow gg \rightarrow q\bar{q}\gamma\gamma$ decrease as $\sqrt{\hat{s}}$ increases. On the contrary, the reducible QCD backgrounds become relatively more important in this high energy region, which are the main backgrounds of our two photon signal.

We calculate the cross sections for the dominant high p_T QCD subprocesses by using PYTHIA [26]. We have applied the basic cuts of $p_T \geq 30$ GeV and $|\eta| \leq 2.44$. The dominant cross sections are

$$\begin{aligned}\sigma(gg \rightarrow gg) &= 6.91 \times 10^8 \text{ pb}, \\ \sigma(qg \rightarrow qg) &= 8.71 \times 10^8 \text{ pb}, \\ \sigma(gg \rightarrow q\bar{q}) &= 1.23 \times 10^7 \text{ pb}.\end{aligned}\tag{34}$$

Other subprocesses have much smaller cross sections. With integrated luminosity of 100 fb⁻¹, the total number of background events is as huge as 1.57×10^{14} .

In order to suppress the QCD background, we first select the photons of $E_\gamma > 50$ GeV in the simulated events and take the most energetic two photons as the photon candidates. Our kinematic cuts are chosen based on the characteristic features of the photons from the background events and the signal: (i) most of the background photons are in the forward and backward directions along the beam line; (ii) two photons of our signal events are in the opposite directions in the partonic c.m. frame. Therefore, we apply kinematic cuts to exclude the forward and backward photons along the beam line, as well as the collinear photons. The following kinematic cuts are called the CUT I:

CUT I (1): Transverse momentum cuts of $p_T > 30$ GeV for both photons are applied.

CUT I (2): We demand that the opening angle of two photons are to be $-1 < \cos \theta < -0.8$.

CUT I (3): No other photons are collinear to the photon candidates, where the collinear photon is defined by $0^\circ < \theta < 20^\circ$.

Having applied CUT I, we reduce the background events by five order of magnitude.

For the next step, we use the longitudinal boost invariance at the LHC. The two photons in our signal have back-to-back momenta in the transverse plane. We apply the following CUT II:

CUT II (1): The magnitudes of the transverse momenta of two photons are same,

$$-0.01 < \frac{p_{1T} - p_{2T}}{p_{1T} + p_{2T}} < 0.01. \quad (35)$$

CUT II (2): The opening angle of the transverse momenta of two photons are in the opposite direction, $-1 < \cos \theta_T < -0.985$.

With the CUT II applied, the background events are reduced by three order of magnitude, leaving 5.4×10^6 events as the SM backgrounds.

Finally we apply the kinematic cut on the invariant mass distribution of two photons. Most QCD background photons have their invariant mass distribution in the low mass region, less than 300 GeV. With both CUT I and CUT II, there are less than 50 events per 10 GeV. On the contrary, our signal $\chi^{(2)} \rightarrow \gamma\gamma$ in the optimal scenario has about 61 events. Therefore we have a very sharp peak over the SM backgrounds.

V. CONCLUSIONS

The probe of massive Higgs bosons with mass above 500 GeV beyond the observed SM particles is an interesting possibility at the LHC. Within the SM, the Higgs boson can be that heavy. In the MSSM, additional heavy CP-even and CP-odd neutral Higgs bosons can be good candidates. At the LHC, however, their detection is very challenging. The production of this heavy Higgs boson, mainly through the gluon fusion, is reduced by the kinematic suppression. And the detection is not clean: the SM heavy Higgs boson is too obese ($\Gamma_{h_{SM}} \simeq m_{h_{SM}}$) to clearly declare the observation from the golden $ZZ \rightarrow 4\ell$ mode; in the decoupling limit the MSSM heavy neutral Higgs bosons mainly decay into $t\bar{t}$ and $b\bar{b}$ for the small and large $\tan\beta$ case, respectively, which suffer from the QCD backgrounds.

We found that the second KK modes of the Higgs boson in the mUED model are also very interesting candidates for massive Higgs bosons. And they have very distinctive features from the heavy Higgs bosons in the SM and MSSM. Highly degenerate mass spectrum within

the given KK level closes kinematically most of the KK-number-conserving decays into the first KK modes. This kinematic closure leads to quite distinctive phenomenology compared with the heavy Higgs boson(s) in the SM and MSSM. First their total decay width is much small, which leads to a sharp resonance at the LHC. The second characteristic is the large branching ratio of CP-odd $\chi^{(2)}$ decay into two photons or two gluons.

It is also remarkable that $h^{(2)} \rightarrow gg, \gamma\gamma$ through the KK fermion (mainly top) loops is prohibited since the coupling of the CP-even second KK Higgs boson with the first KK fermions are off-diagonal. The $h^{(2)}$ production through the gluon fusion is not feasible at the LHC. On the contrary, the CP-odd $\chi^{(2)}$ has diagonal Yukawa couplings, though suppressed by the factor of m_t/M_1 . Both $\chi^{(2)} \rightarrow gg$ and $\chi^{(2)} \rightarrow \gamma\gamma$ are allowed at one-loop level. The CP-odd $\chi^{(2)}$ can be produced through the gluon fusion. With the sizable $\text{BR}(\chi^{(2)} \rightarrow \gamma\gamma)$, the resonance in the $\gamma\gamma$ invariant mass distribution gives a clear probe of the mUED model.

ACKNOWLEDGMENTS

This work is supported by WCU program through the KOSEF funded by the MEST (R31-2008-000-10057-0). KYL is also supported by the Basic Science Research Program through the National Research Foundation of Korea (NRF) funded by the Korean Ministry of Education, Science and Technology (2009-0076208). SC is supported by the Basic Science Research Program through the NRF funded by the Korean Ministry of Education, Science and Technology (KRF-2008-359-C00011). SC thanks KIAS for warm support during his visit.

-
- [1] T. Appelquist, H. C. Cheng and B. A. Dobrescu, Phys. Rev. D **64**, 035002 (2001) [arXiv:hep-ph/0012100].
 - [2] T. Appelquist, B. A. Dobrescu, E. Ponton and H. U. Yee, Phys. Rev. Lett. **87**, 181802 (2001) [arXiv:hep-ph/0107056].
 - [3] B. A. Dobrescu and E. Poppitz, Phys. Rev. Lett. **87**, 031801 (2001) [arXiv:hep-ph/0102010].
 - [4] I. Antoniadis, Phys. Lett. B **246**, 377 (1990).
 - [5] H. C. Cheng, J. L. Feng and K. T. Matchev, Phys. Rev. Lett. **89**, 211301 (2002) [arXiv:hep-ph/0207125].

- [6] H. C. Cheng, K. T. Matchev and M. Schmaltz, Phys. Rev. D **66**, 036005 (2002) [arXiv:hep-ph/0204342].
- [7] T. G. Rizzo, Phys. Rev. D **64**, 095010 (2001) [arXiv:hep-ph/0106336]. C. Macesanu, C. D. McMullen and S. Nandi, Phys. Rev. D **66**, 015009 (2002) [arXiv:hep-ph/0201300]. K. Agashe, N. G. Deshpande and G. H. Wu, Phys. Lett. B **514**, 309 (2001) [arXiv:hep-ph/0105084]. T. Appelquist and B. A. Dobrescu, Phys. Lett. B **516**, 85 (2001) [arXiv:hep-ph/0106140].
- [8] A. J. Barr, Phys. Lett. B **596**, 205 (2004) [arXiv:hep-ph/0405052].
- [9] A. Datta, K. Kong and K. T. Matchev, Phys. Rev. D **72**, 096006 (2005) [Erratum-ibid. D **72**, 119901 (2005)] [arXiv:hep-ph/0509246].
- [10] H. C. Cheng, K. T. Matchev and M. Schmaltz, Phys. Rev. D **66**, 056006 (2002) [arXiv:hep-ph/0205314].
- [11] F. J. Petriello, JHEP **0205**, 003 (2002) [arXiv:hep-ph/0204067].
- [12] B. Bhattacharjee and A. Kundu, Phys. Lett. B **653**, 300 (2007) [arXiv:0704.3340 [hep-ph]].
- [13] A. Datta, K. Kong and K. T. Matchev, New J. Phys. **12**, 075017 (2010) arXiv:1002.4624 [hep-ph].
- [14] G. Belanger, M. Kakizaki, A. Pukhov, [arXiv:1012.2577 [hep-ph]].
- [15] A. Djouadi, Phys. Rept. **457**, 1 (2008) [arXiv:hep-ph/0503172], Phys. Rept. **459**, 1 (2008). [hep-ph/0503173].
- [16] P. H. Chankowski, S. Pokorski, J. Rosiek, Nucl. Phys. **B423**, 437-496 (1994); P. H. Chankowski, S. Pokorski, J. Rosiek, Nucl. Phys. **B423**, 497-531 (1994).
- [17] I. Gogoladze, C. Macesanu, Phys. Rev. **D74**, 093012 (2006). [hep-ph/0605207].
- [18] U. Haisch, A. Weiler, Phys. Rev. **D76**, 034014 (2007). [hep-ph/0703064 [HEP-PH]].
- [19] S. Arrenberg, L. Baudis, K. Kong, K. T. Matchev, J. Yoo, Phys. Rev. **D78**, 056002 (2008); S. Matsumoto, J. Sato, M. Senami, M. Yamanaka, Phys. Rev. **D80**, 056006 (2009). [arXiv:0903.3255 [hep-ph]]. B. Bhattacharjee, M. Guchait, S. Raychaudhuri, K. Sridhar, Phys. Rev. **D82**, 055006 (2010). [arXiv:1006.3213 [hep-ph]].
- [20] ATLAS Collaboration, Report No. ATL-PHYS-PUB-2009-053.
- [21] See, *i.e.*, M. Cacciari, S. Frixione, M. L. Mangano, P. Nason, G. Ridolfi, JHEP **0809**, 127 (2008) and references therein.
- [22] A. D. Martin, R. G. Roberts, W. J. Stirling *et al.*, Eur. Phys. J. **C14**, 133 (2000). [hep-ph/9907231].

- [23] D. E. Kaplan, K. Rehermann, M. D. Schwartz and B. Tweedie, *Phys. Rev. Lett.* **101**, 142001 (2008) [arXiv:0806.0848 [hep-ph]].
- [24] B. Bhattacharjee, M. Guchait, S. Raychaudhuri and K. Sridhar, *Phys. Rev. D* **82**, 055006 (2010) [arXiv:1006.3213 [hep-ph]].
- [25] V. Barger and R.J.N. Phillips, *Collider Physics* (Addison-Wesley, 1987).
- [26] T. Sjostrand, S. Mrenna and P. Z. Skands, *JHEP* **0605**, 026 (2006) [arXiv:hep-ph/0603175].